Hadron energy response of the ICAL detector at INO

Moon Moon Devi[1*], Anushree Ghosh[2†], Daljeet Kaur[3‡], Lakshmi S. Mohan[4§], Sandhya Choubey[2], Amol Dighe[1], D. Indumathi[4], Sanjeev Kumar[3], M. V. N. Murthy[4], Md. Naimuddin[3]

[1] *Tata Institute of Fundamental Research, Mumbai 400 005, India*
[2] *Harishchandra Research Institute, Allahabad 211 002, India*
[3] *Department of Physics & Astrophysics, University of Delhi, Delhi 110 007, India*
[4] *The Institute of Mathematical Sciences, Chennai 600 113, India*

April 19, 2013

Abstract

We present results of a Monte Carlo simulation study of the hadron energy response (for 1 GeV $\leq$ E $\leq$ 15 GeV) of the magnetized iron calorimeter detector, ICAL, proposed to be located at the India-based Neutrino Observatory. Using a GEANT4 modeling of the ICAL, interactions of atmospheric neutrinos with target nuclei are recorded. We discuss a method of calibration of the hadron energy using the hadron hit multiplicity in the active detector element. We first study the detector response with single pions propagating through the detector. Then the average response of hadrons produced in atmospheric neutrino interactions is analyzed using NUANCE-generated neutrino events. The shape of the distribution and an appropriate fitting function are examined in detail. Finally, the hadron energy resolution is determined as a function of energy. We find an energy resolution of around (60–40)% for hadron energies in the range 2–15 GeV.

*moonmoon4u@tifr.res.in
†anushree@hri.res.in
‡daljeet.kaur97@gmail.com
§slakshmi@imsc.res.in

1 Introduction

The India-based Neutrino Observatory (INO) [1] is a planned underground laboratory in South India with the long term goal of conducting experiments on cosmic rays, neutrinos and astrophysics. The primary focus of INO in the first phase is the study of atmospheric neutrinos with a magnetized iron calorimeter (ICAL) detector similar in concept to the design of the MONOLITH detector [2]. The detector is designed to observe neutrino (and anti-neutrino) interactions in the GeV range. The main aim of the ICAL detector is a precise measurement of the oscillation parameters both for neutrinos and anti-neutrinos; recent measurements of the mixing angle θ_{13} in reactor experiments [3] [4] [5] will enable the ICAL to pin down the mass ordering of neutrinos by separate measurements of ν_μ and $\bar{\nu}_\mu$ interactions by exploiting matter effects in the earth.

The specifications of the magnetized ICAL detector, consisting of three identical modules with layers of iron plates interspersed with resistive plate chamber (RPC) detectors and approximately 50 kton in mass, are given in Table 1. RPC detectors have been chosen as the active detector elements by virtue of their good position (cm) and timing (ns) resolution, high detection efficiency for charged particles, long term stability, and coverage of substantial area. The RPC readout strip width for the present simulation study has been assumed as 1.96 cm. ICAL is expected to have good charge identification efficiency and good tracking and energy resolution, especially for muons produced in charged current (CC) interactions of the detector material with atmospheric muon neutrinos. A schematic illustration of the detector is shown in Fig. 1.

No. of modules	3
Module dimension	16 m $\times$ 16 m $\times$ 14.5 m
No. of RPC layers	150
Iron plate thickness	5.6 cm
RPC unit dimension	1.84 m $\times$ 1.84 m$\times$ 24 mm
Total no. of RPC units	28800

Table 1: ICAL detector specifications.

Atmospheric neutrinos (antineutrinos) interact with the iron target in the detector through quasi-elastic (QE), resonance (RS) and deep inelastic scattering (DIS) processes as shown in Table 2, where l is the charged lepton, N, N' are nucleons, while X denotes any set of possible final hadrons, with typically one pion and a nucleon in RS, and multiple hadrons in DIS interactions. At these energies, coherent interactions and the interactions with the electrons in the detector are rare and are ignored.

In this paper, we are concerned mainly with the charged current interactions in which, apart from a muon, there will be hadrons in the final state. While the final state muon in the charged-current ν_μ interaction is reconstructed well for its energy and direction, the hadrons in the final state are observed mainly as a bunch of hits close to the interaction vertex. The physics analysis crucially depends on the precision with which the neutrino energy is reconstructed, and hence on the precision of reconstruction of the energies of the hadrons and muon. The hadrons consist mainly of pions (about

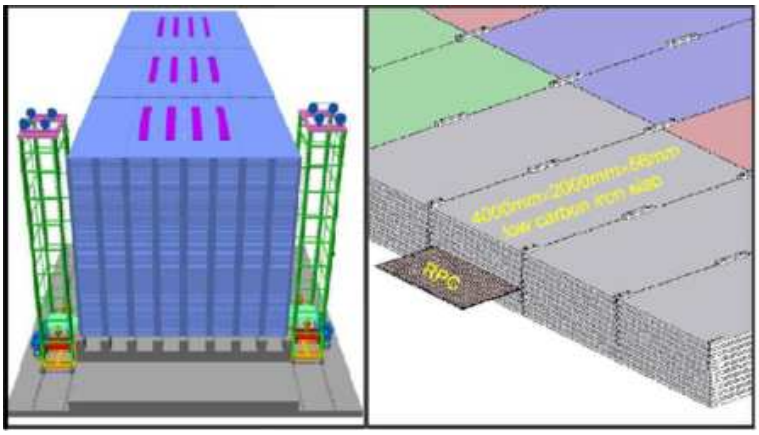

Figure 1: Left: Schematic of ICAL detector. Right: a close up view of the stack and RPC insertion method is shown.

Processes	CC	NC
QE	$\overset{(-)}{\nu}_l N \to l^{\overset{(+)}{-}} N'$	$\overset{(-)}{\nu}_l N \to \overset{(-)}{\nu}_l N'$
RS & DIS	$\overset{(-)}{\nu}_l N \to l^{\overset{(+)}{-}} X$	$\overset{(-)}{\nu}_l N \to \overset{(-)}{\nu}_l X$

Table 2: The neutrino interaction processes.

85% of events on the average), kaons, and also nucleons, including the recoil nucleon which cannot be distinguished from the remaining hadronic final state. Both neutral and charged pions may be produced. The neutral pion decays immediately, giving rise to two photons, while the charged pions propagate and develop into a cascade due to strong interactions. The main uncertainty in determining the incident neutrino energy comes from the uncertainty in estimating the energy of these hadrons. Typically a muon leaves a distinct track whereas the hadrons leave a shower of hits close to the vertex. A visualization of a neutrino DIS event with large hadron energy component in the simulated ICAL detector (using the VICE event display package [6]) is shown in Fig. 2. For the interaction $\nu_\mu N \to \mu X$, the incident neutrino energy is given by

$$\mathrm{E}_\nu = \mathrm{E}_\mu + \mathrm{E}'_{\mathrm{had}}, \tag{1}$$

where $\mathrm{E}'_{\mathrm{had}}$ is the difference in the total energy of the final state hadrons (including the recoil nucleon) and the energy of the initial state nucleon — including the rest mass, Fermi momentum and binding energy. We use $\mathrm{E}'_{\mathrm{had}}$ as an observable for hadron energy since it would enable us to reconstruct the neutrino energy in a straightforward manner.

The analysis is done in two parts. Mono-energetic charged pions are propagated through the detector and their characteristics studied. These are used to determine a suitable probability distribution function (PDF) at each energy. Next, we consider hadrons produced through neutrino interactions. Here in principle all types of hadrons contribute to the energy, though it is dominated by pions at the energies of a few GeV. $\mathrm{E}'_{\mathrm{had}}$ can be reconstructed in ICAL by devising a calibration with respect to the number

of hits in a hadron shower. In general the energy resolution of hadrons is affected by various factors like shower energy fluctuation, leakage of energy and invisible energy loss mechanisms.

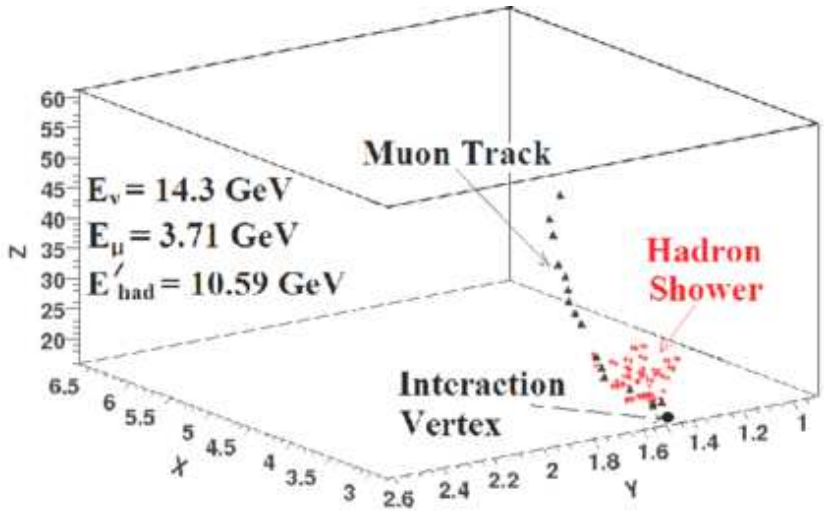

Figure 2: A deep inelastic neutrino interaction event in the simulated ICAL detector using VICE event display package.

In this paper we use a full simulation of the event propagation in ICAL to assess the detector's capability to estimate hadron energy. In section 2, we first discuss the hit distributions of hadrons in the detector. This is done by a Monte-Carlo (MC) generator that generates hadrons at fixed energies up to 15 GeV. The hits are are estimated using the hit multiplicity information of events generated with appropriate position- and angle-smearing. We then specifically discuss the pion energy (E_π) resolution by propagating pions with fixed energies through the simulated detector, focusing on the appropriate pdf to be used for analyzing the pion hits. In section 3, we use the hadrons (not just pions) generated in atmospheric neutrino-nucleus interactions using a neutrino event generator NUANCE [9], and study the net hadron energy resolution as a function of E'_{had}. In section 4, we discuss the calibration of E'_{had} using the hit information. We conclude in section 5.

2 Energy resolution with fixed energy pions

The ICAL detector, with the parameters specified in Table 1, is simulated using the GEANT4 package [7, 8]. For more details about the coding of the detector geometry and the nature of hits generated, see Ref. [10]. Our focus in this section will be on the analysis of fixed-energy single-pion hit distributions.

When a charged particle propagates through the ICAL detector, hits in the X and Y strips of the RPC layers are recorded [12]. The layer number provides the z-coordinate. Thus the full position information is available. A muon usually leaves one or two hits per layer and so the hits from both X and Y strips can easily be combined to obtain the

number of hits and their position coordinates (x, y) in a given layer. However, in the case of hadron shower there are multiple hits per layer, and combining X and Y strip hits leads to some false count of hits (ghost hits). To avoid the ghost hit counts, the energy calibration may be done with counts from either X or Y strips. The variables x-hits and y-hits store the number of hits in the X and Y strips of the RPC, respectively. The maximum of x-hits or y-hits is stored as the variable orig-hits. In Fig. 3, the comparison of these three types of hit variables are shown for $\pi^{\pm}$ of energy 3 GeV. As is clear from Fig. 3, we could have used any of the x-, y-or orig-hits in the analysis; we choose to use orig-hits as the unbiased parameter.

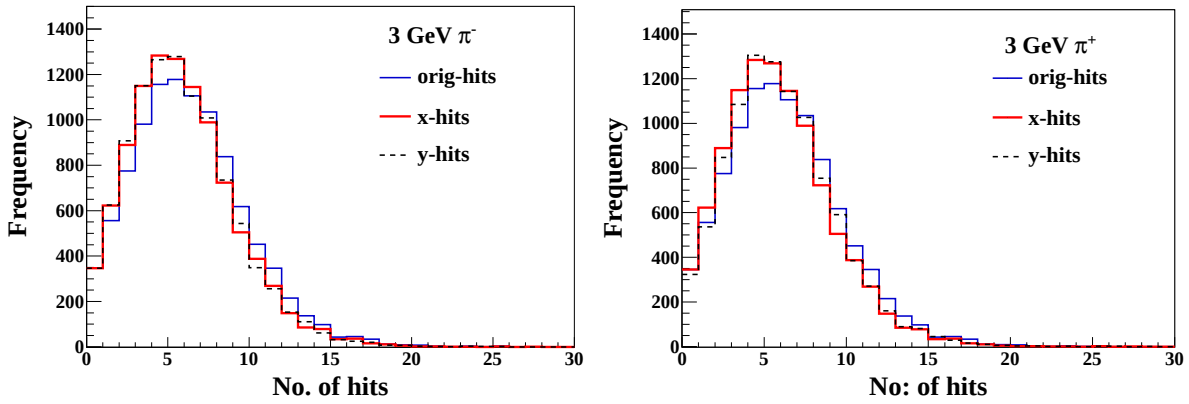

Figure 3: The comparison of the distributions of x-hits, y-hits and orig-hits for (left) π^- and (right) π^+ of energy 3 GeV.

Unless otherwise specified in this section, the total number of events for each input energy value is 10000. Each event is randomly generated over a volume 200 cm $\times$ 200 cm $\times$ 200 cm in the central region of the ICAL detector. In addition, since there is very little impact of the magnetic field on the showers produced by hadrons, the hadron direction is uniformly smeared over zenith angle $0 \leq \theta \leq \pi$ and azimuth of $0 \leq \phi \leq 2\pi$. The angles are denoted with respect to a reference frame, where the origin is taken to be the center of the detector, the z-axis points vertically up, while the plates are horizontal in the x-y plane. This serves to smear out any angle-dependent bias in the energy resolution of the detector by virtue of its geometry which makes it the least (most) sensitive to particles propagating in the horizontal (vertical) direction.

In Fig. 4 the hit distributions in the detector for pions, kaons, and protons at various energies in the range of 1 to 15 GeV are shown. We observe that for all these hadrons the hit patterns are similar, though the peak position and spread are somewhat dependent on the particle. The detector cannot distinguish the specific hadron that has generated the shower. Since hadrons produced in neutrino interactions with ICAL are primarily charged pions, we focus our attention on the detector response to pions in this section and consider a more general admixture of different hadrons in Section 3. However, since the energy response of all hadrons appears to be rather similar, there should be no significant information loss even when we cannot identify the final state hadrons.

We will therefore use the hit distribution of charged pions at various energies to

determine the detector response. In particular we determine the mean and variance of the distribution and their energy dependence. Later on we will discuss a suitable probability distribution function for the hit patterns generated. This information is required in order to determine the energy calibration for use in physics studies with ICAL.

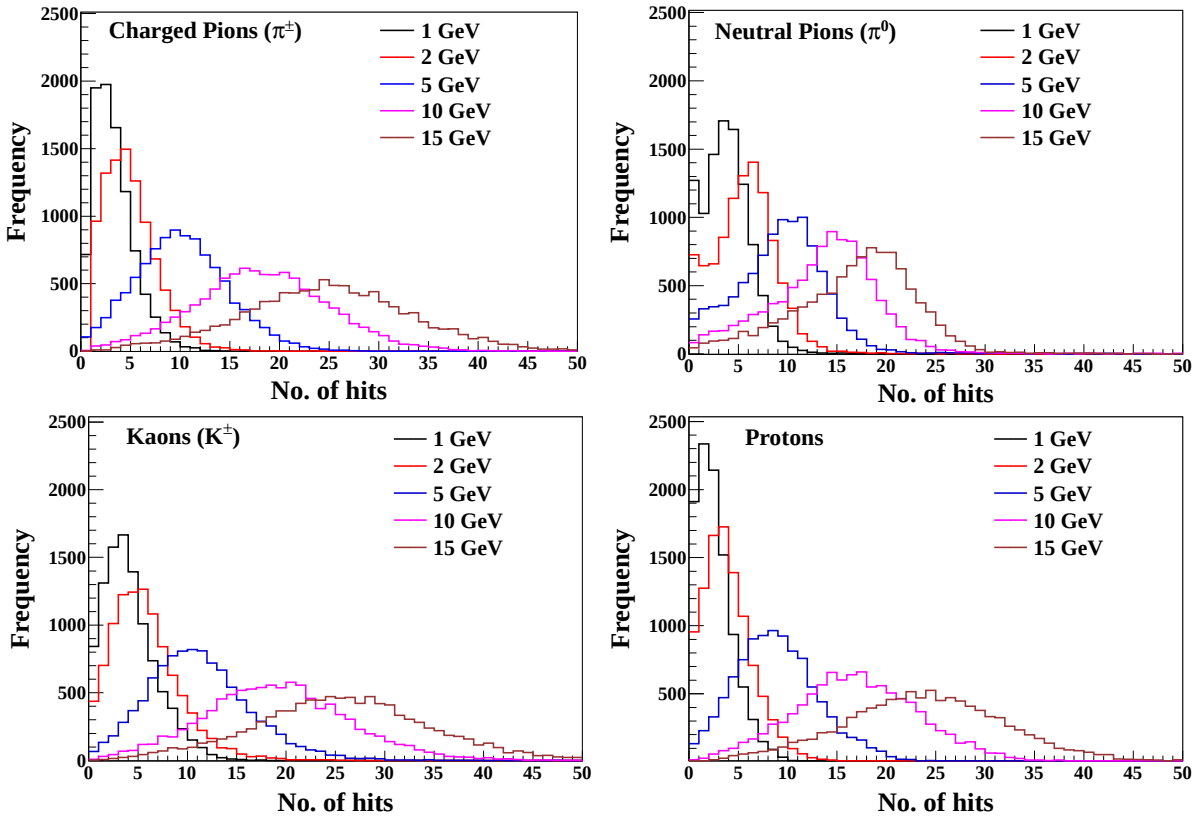

Figure 4: The hit distributions at various energies (angle averaged) for $\pi^{\pm}$, π^0, $K^{\pm}$ and protons propagated from vertices smeared over the chosen volume.

2.1 Analysis of the pion ($\pi^{\pm}$) hit pattern

The pion hit distributions at sample values of E = 3, 8 GeV are shown in Fig. 5, where the arithmetic mean and rms value obtained from the histogram are also listed. Typical patterns show a mean of roughly 2 hits per GeV as seen from the figure, but with long tails, so the distribution is not symmetric. In addition, several events yield zero hits in the detector at lower energies, such events are virtually absent at higher energies.

Fig. 5 also shows the fits to the Gaussian distribution. As can be seen from the figure, the quality of the fit at the lower energy (E = 3 GeV) is poor, with a χ^2 per degree of freedom, $\chi^2/\text{ndf} \approx 4.6$. This improves to $\chi^2/\text{ndf} \approx 2.2$ for E = 8 GeV. This clearly indicates that the hit pattern is non-Gaussian for lower energy pions. This is also easily understood because of the long non-Gaussian tails. However, at high energies the hit distribution is well approximated by a Gaussian.

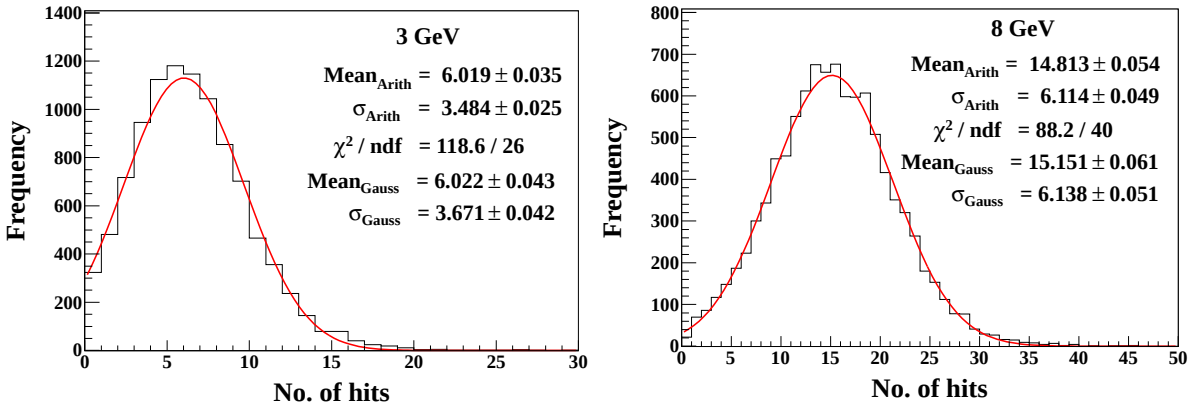

Figure 5: The hit distributions at 3 GeV (left) and 8 GeV (right), for pions propagated from randomized vertices over a volume of 200 cm × 200 cm × 200 cm in the detector. A Gaussian fit to the histogram is included for later convenience.

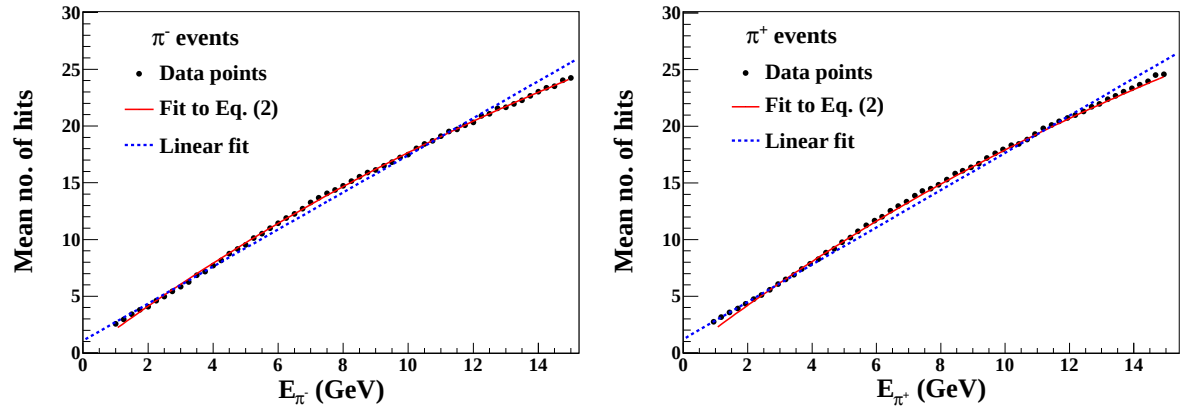

Figure 6: Mean hit distribution as a function of pion energy with 5.6 cm iron plates. Left (right) panel shows the mean hit for π^- (π^+). Black dots are the results of simulation while the curves are fits to this simulated data.

The arithmetic mean $\bar{n}(\mathrm{E})$ of the number of hits increases with increasing pion energy, and saturates at higher energies. It may be approximated by

$$\bar{n}(\mathrm{E}) = \mathrm{n_0}[1 - \exp(-\mathrm{E}/\mathrm{E_0})], \tag{2}$$

where $\mathrm{n_0}$ and $\mathrm{E_0}$ are constants. This fit has to be used with some care, since $\mathrm{n_0}$ and $\mathrm{E_0}$ are sensitive to the energy ranges of the fit. In Fig. 6, we compare the means of the hit distributions for π^- and π^+ events in the detector, in the energy range 1 – 15 GeV. We also show the fits to Eq. (2). As expected, the mean number of hits for π^- and π^+ are identical within expected statistical fluctuations. The value of $\mathrm{E_0}$ is found to be ~ 30 GeV. Since the energies of interest for atmospheric neutrinos are much less than E_0, we may use Eq. (2) in its approximate linear form $\bar{\mathrm{n}}(\mathrm{E}) = \mathrm{n_0 E}/\mathrm{E_0}$. Fig. 6 also shows a fit to this linear form.

In the linear regime ($E \ll E_0$), we have

$$\frac{\bar{n}(E)}{n_0} = \frac{E}{E_0}, \tag{3}$$

and therefore the energy resolution may be written as

$$\frac{\sigma}{E} = \frac{\Delta n(E)}{\bar{n}(E)}, \tag{4}$$

where Δn is the RMS width of the distribution. In the rest of the paper we shall use the notation σ/E for energy resolution, and use Eq. (4) for the rest of the analysis.

The energy resolution of pions may be parametrized by

$$\frac{\sigma}{E} = \sqrt{\left(\frac{a}{\sqrt{E}}\right)^2 + b^2}\ , \tag{5}$$

where a and b are constants. In the literature a is often referred to as the stochastic coefficient which incorporates both statistical and systematic uncertainties. In Fig. 7, we show the π^- and π^+ energy resolutions as functions of pion energy, and extract the parameters a and b by a fit to Eq. (5) over the energy range 1–15 GeV. It is seen that while the fits to both π^- and π^+ yield virtually identical values for a and b, the quality of fits is rather poor at low energies.

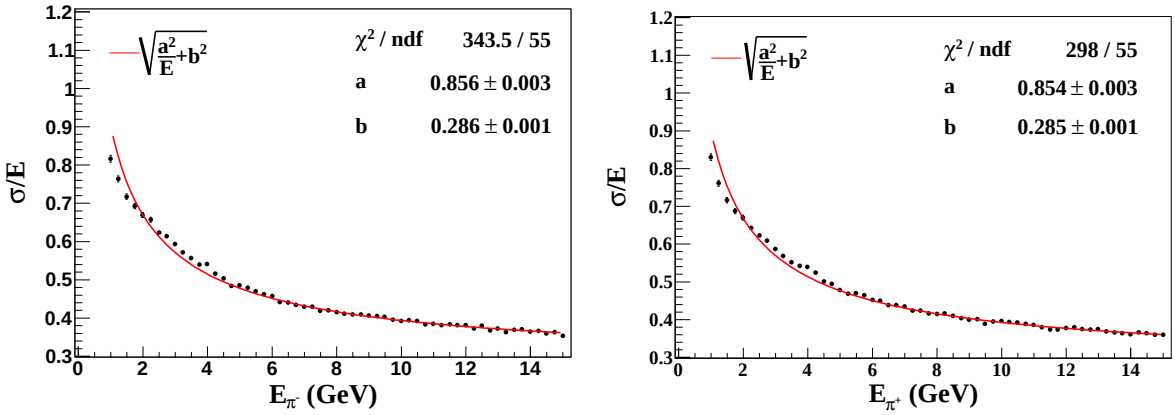

Figure 7: Energy resolutions for π^- (left) and π^+ (right) for different energies shown as a function of pion energy. Also shown is the fit to this resolution according to Eq. (5).

As observed in this section, the Gaussian distribution is not a good approximation at low energies, while, it approximates the hit distribution well at higher energies. It is desirable to find a suitable fit function that correctly reproduces the mean and variance at all energies, and is well-approximated by a Gaussian distribution at higher energies. We shall do so in the next section.

2.2 A suitable probability distribution function

From Fig. 4, it is clear that the hit distribution approaches the Gaussian pdf only at energies greater than around 5 GeV. Since the bulk of atmospheric neutrino events, the ones that ICAL detector will record, are concentrated in the energy range less than about 10 GeV, it becomes important to find a suitable pdf for the hit distribution. This should necessarily agree with the Gaussian pdf at high energies. We consider this question in detail in this section.

Here we analyze the hit distributions using three fitting functions. As we have seen, the hit distribution is asymmetric, particularly at lower energies. We therefore compare the following functional forms: (i) Gaussian, (ii) Landau convoluted with a Gaussian, and (iii) Vavilov [11]. The energy loss of a particle passing through moderately thick absorbers is commonly modelled using the above three distributions depending on the energy of interest.

In Fig. 8, we show the sample hit distributions for 10000 pions propagated through the detector from randomised vertex points, at sample energies of 3 GeV and 8 GeV, fitted to the three functional forms. A comparison of the fit parameters is shown in Table 3, where we also indicate the P-values obtained from the Kolmogorov-Smirnov (KS) test. It is clear that the best fit is obtained with the Vavilov pdf. A sweep of all other energies shows that the Vavilov pdf consistently gives a better fit than the other distributions. This is what we will use in the analysis that follows from now on. We however note that even though the χ^2 differs substantially, the mean and σ obtained from different fits are quite similar. We shall quantify this in section 2.4.

E_π	Parameters	Histogram	Gaussian	Landau	Vavilov
3 GeV	χ^2/ndf		4.6	4.2	1.7
	P (KS test)		8.1×10^{-6}	7.6×10^{-6}	0.95
	$\bar{n}$	6.019	6.022±0.043	6.021±0.043	6.018±0.044
	σ	3.484	3.671±0.042	3.601±0.048	3.431±0.052
8 GeV	χ^2/ndf		2.204	2.01	1.607
	P (KS test)		2.6×10^{-4}	1.2×10^{-4}	0.92
	$\bar{n}$	14.813	15.151±0.061	15.062±0.063	14.781±0.063
	σ	6.114	6.138±0.051	6.129±0.053	6.124±0.068

Table 3: Comparison of the three different pdf fits for 3 GeV and 8 GeV pions. The χ^2 values as well as the Kolmogorov-Smirnov (KS) statistics quantify the substantial differences in the quality of fits with different pdfs. Note that the mean and sigma are less sensitive to the choice of pdf. For comparison the mean and rms obtained directly from the hit distribution are also shown in the third column.

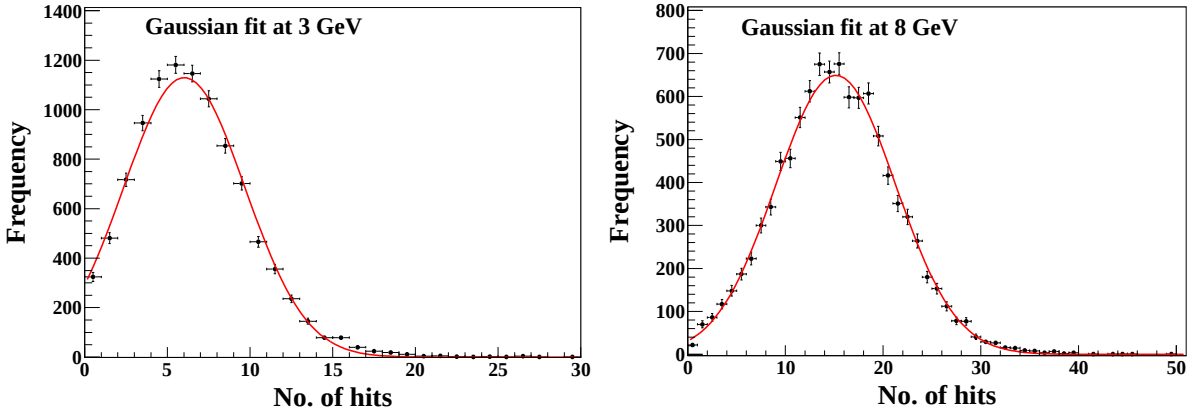

(a)

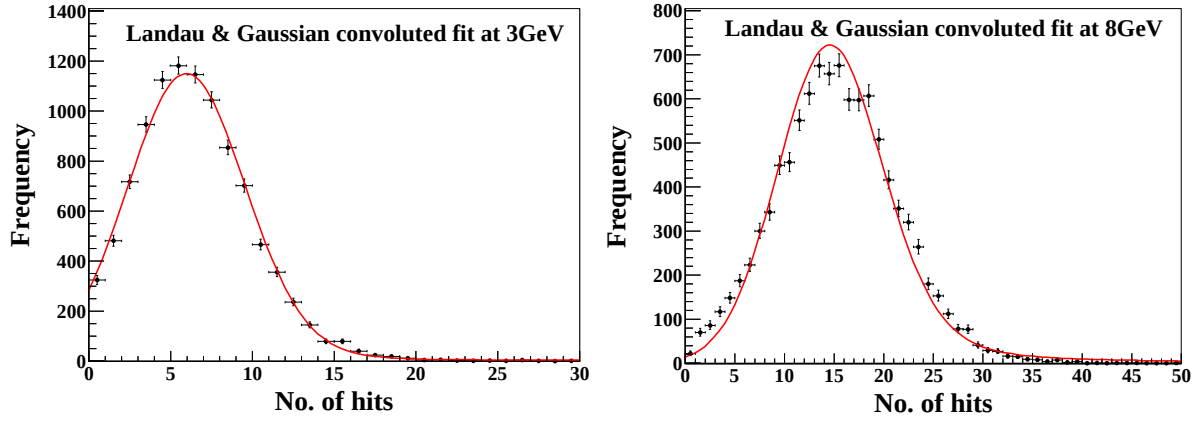

(b)

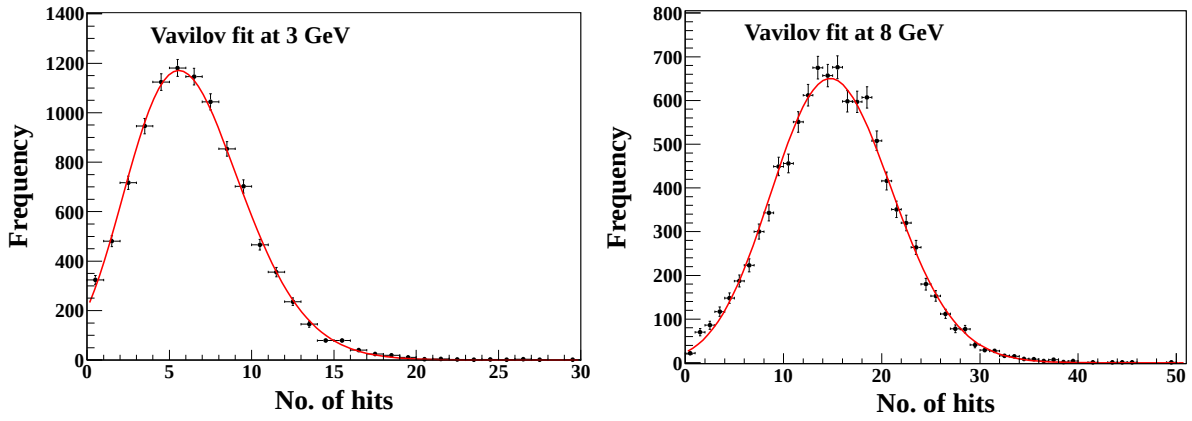

(c)

Figure 8: The hit distributions at sample energies 3 GeV and 8 GeV, shown with statistical errors and fitted with (top) Gaussian, (middle) Landau convoluted with Gaussian, and (bottom) Vavilov distributions. The resulting fit parameters and quality of fits are shown in Table 3.

2.3 Energy resolution using the Vavilov fit

We now parameterize the energy resolution of pions using the Vavilov fit, which has four parameters, P_0, P_1, P_2 and P_3 (see Appendix A for details). In Fig. 9, we show the variation of the Vavilov parameters P_0, P_1, P_2, P_3 with pion energy. The mean and σ are obtained from these parameters via

$$\text{Mean} = (\gamma \ - \ 1 \ - \ \ln P_0 - P_1)\ P_3 + P_2; \qquad \sigma^2 = (2 - P_1)\ \frac{P_3^2}{2P_0}, \tag{6}$$

where γ is the Euler's constant. The main features of the Vavilov distribution may be captured by the two parameters mean and sigma. However the remaining information in the Vavilov parameters enables a good fit even in the regions of low hit multiplicity and the tail of high hit multiplicity.

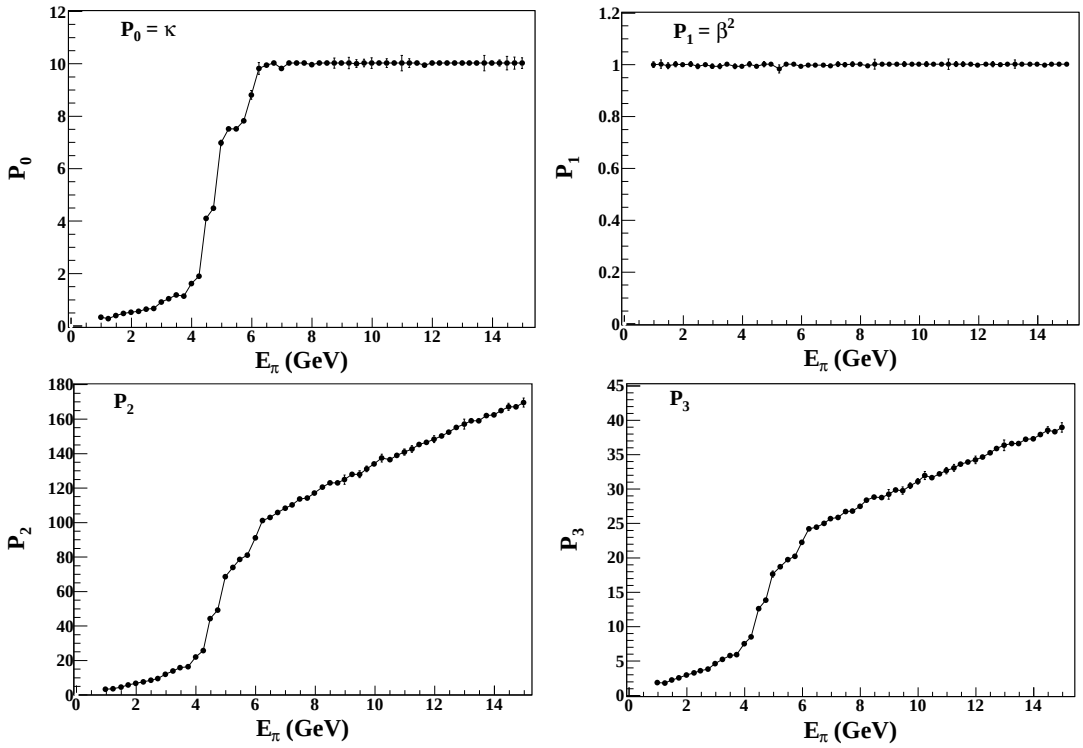

Figure 9: Variation of the Vavilov fit parameters P_0, P_1, P_2, and P_3 with pion energy. Notice that beyond E $\sim$ 6 GeV, we have $P_0 \simeq 10$, so that the Vavilov distribution reduces to a Gaussian.

Note that for $P_0 \gtrsim 10$, Vavilov distribution reduces to a Gaussian pdf with the corresponding mean and σ. In this analysis this happens for energies greater than $\sim$ 6 GeV. The actual power of Vavilov distribution is therefore apparent in the energy range 1–6 GeV, which is the main region of interest for hadrons in the ICAL detector.

Thus having extracted the mean and σ as discussed above, in Fig. 10 we plot the resolution σ/E as a function of energy. This is then fitted to Eq. (5) to obtain the coefficients a and b. The fit has been done separately for the energy ranges 1–5 GeV,

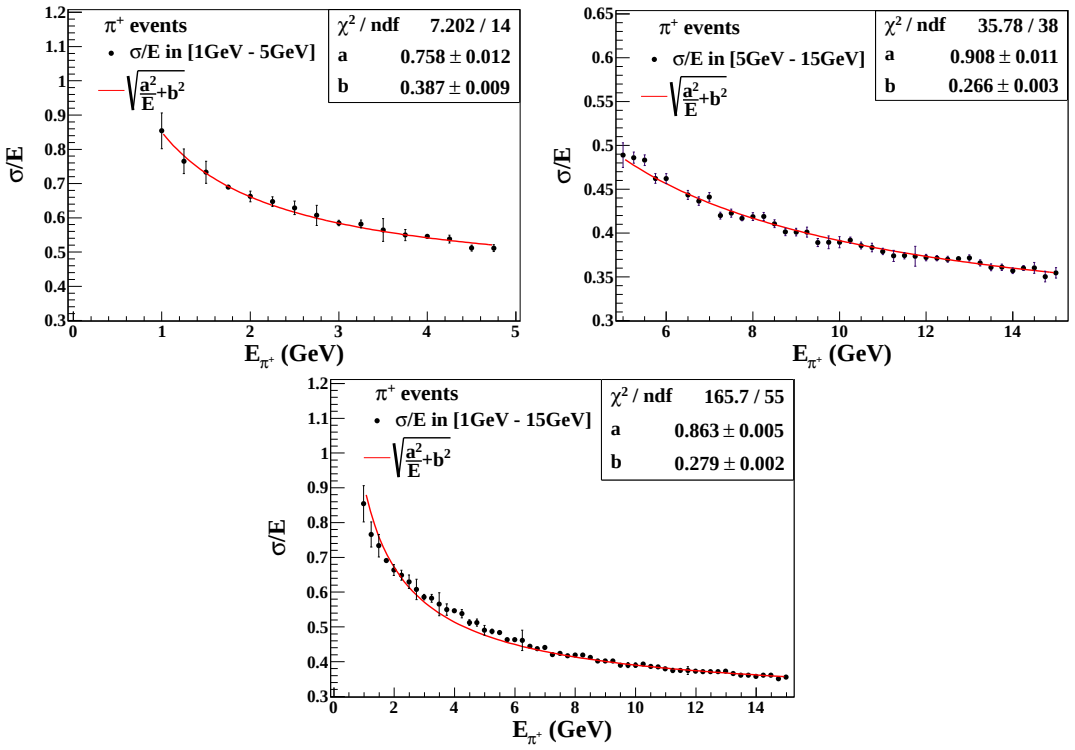

Figure 10: Resolution σ/E plotted using the Vavilov fit for as a function of energy. The resolution is fitted to Eq. (5) in three different energy ranges as shown.

5–15 GeV, and the combined energy range 1–15 GeV. The low energy region (1–5 GeV) is the region where Vavilov pdf gives the best fit, while the Gaussian distribution fails.

2.4 Comparison of the means and σ's for different pdfs

Before we conclude the analysis of fixed energy single pion events, a few remarks are in order about the various fits used. Though the Vavilov distribution gives a good fit to the data, it has four correlated parameters, as opposed to the two parameters $\text{mean}_{\text{Gauss}}$ and σ_{Gauss} in the Gaussian pdf. To a first approximation the $\text{mean}_{\text{Vavilov}}$ and σ_{Vavilov} are sufficient to determine the energy resolution. Often, for some applications, for example where detector parameters are checked for performance, a simpler alternative may be to use the fit-independent parameters $\text{mean}_{\text{Arith}}$ and σ_{Arith}, the arithmetic mean and the rms width, respectively. In Fig. 11, the mean and σ obtained directly from the hit distribution is compared with those obtained from the Gaussian and Vavilov distributions.

The plots in Fig. 11 show that $\text{mean}_{\text{Arith}}$ and the means obtained from the distributions are comparable with marginal differences. However, the comparison of σ's shows that at low energies σ_{Gauss} deviates from (and is higher than) σ_{Arith}. This can be clearly seen in Fig. 12, where the ratios of the fitted mean and σ with respect to the corresponding fit-independent values are plotted as functions of energy. The marginally higher value of $\text{mean}_{\text{Gauss}}$ as compared to $\text{mean}_{\text{Arith}}$ at higher energies is the result of the long tail in the hit distribution histogram. Also σ_{Gauss} exceeds the others at lower

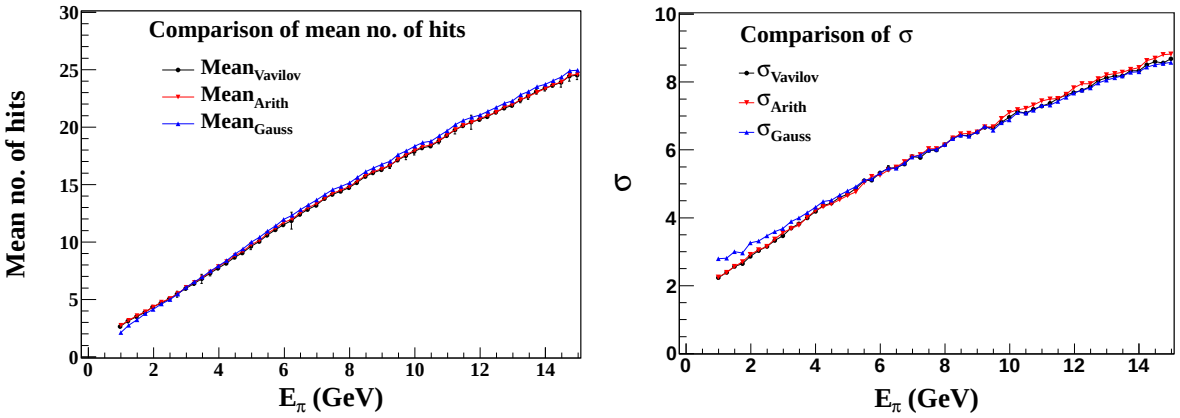

Figure 11: The comparison of mean (left) and σ (right) obtained from the Vavilov and Gaussian pdfs, as well as the fit-independent quantities.

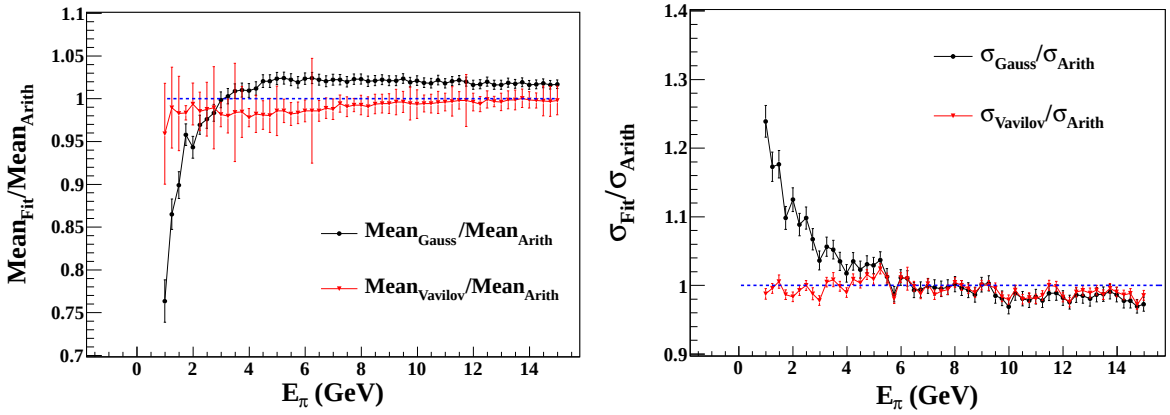

Figure 12: The ratio of mean and σ from Vavilov and Gaussian distributions to $\text{mean}_{\text{Arith}}$ and σ_{Arith}.

energies because of the many events with zero hits at lower energies. Interestingly, at higher energies, while σ_{Gauss} and σ_{Vavilov} agree, they marginally underestimate the σ_{Arith}. This is again due to the presence of the tail. While care is required at low energies, the resolution is fairly distribution independent for higher energies, beyond 6 GeV.

3 Energy resolution with NUANCE-generated neutrino events

The previous section contained an analysis of the energy resolution with single pion events. In actual practice we are interested in the energy resolution of hadrons produced through atmospheric neutrino interactions. In this section, we analyze the energy resolution of hadrons produced in charged-current (CC) atmospheric ν_μ interactions in the detector. Both atmospheric neutrino (ν_μ) and anti-neutrino ($\overline{\nu}_\mu$) events in ICAL are generated using the neutrino event generator NUANCE (v3.5) [9]. Though these are

mainly pions, there are some events with kaons (about 10%) and other hadrons. There are in general multiple hadrons, especially in the DIS events. As discussed earlier, it is not possible to distinguish among different hadrons from the "hadron shower" seen in the hit pattern. However, since the hit distribution of various hadrons are similar to each other (see Fig. 4), and the NUANCE generator is expected to produce an approximately correct mixture of different hadrons at all energies, it is enough to determine the hadron energy resolution at ICAL through an average of NUANCE events, without having to identify the hadrons individually.

The analysis is done with 1000 kt-years of data (equivalent to 20 years of exposure with the 50 kton ICAL module). The events are angle-averaged and binned in the hadron energy $E'_{had} = E_\nu - E_\mu$. The hit distributions (of the variable orig-hits) are analyzed as before, in each energy bin, averaged over all angles. We show the $\text{mean}_{\text{Arith}}$ and σ_{Arith} of these distributions in Fig. 13. As expected, these are similar to the mean and σ obtained earlier with fixed energy pions. Note that while the energy is kept fixed to a single value in the latter case, the events are binned in energy in the NUANCE-based analysis. Since the mean hits grow approximately linearly with energy, we use the same linearized approximation as before to obtain the energy resolution $\sigma/E = \Delta n/n$.

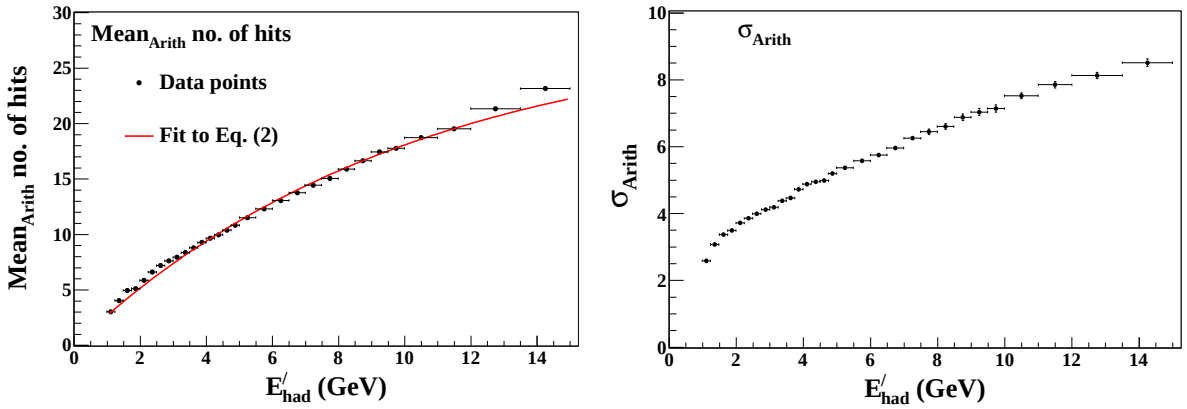

Figure 13: $\text{Mean}_{\text{Arith}}$ and σ_{Arith} of the hit distribution as a function of hadron energy E'_{had}. The bin widths are indicated by the horizontal error bars.

3.1 Analysis of the hit distribution

Now we use the Vavilov distribution function as a fit to the hit distribution of hadrons. The hit distributions and their Vavilov pdf fits for selected energy ranges are shown in Fig. 14. While performing the fit, we use the central value of E'_{had}.

In Fig. 15 we show the energy dependence of the parameters P_0, P_1, P_2, and P_3 of the Vavilov distribution (see Appendix A for details on these parameters) obtained from the fits to the NUANCE data. It can be seen that these results are similar to the fits obtained from the single pion analysis. The changes, mainly a small increase in P_0, P_2 and P_3 at energies $\lesssim 6$ GeV, are primarily because the hadrons in a bin do not have identical energies like the fixed-energy pions in the earlier analysis did.

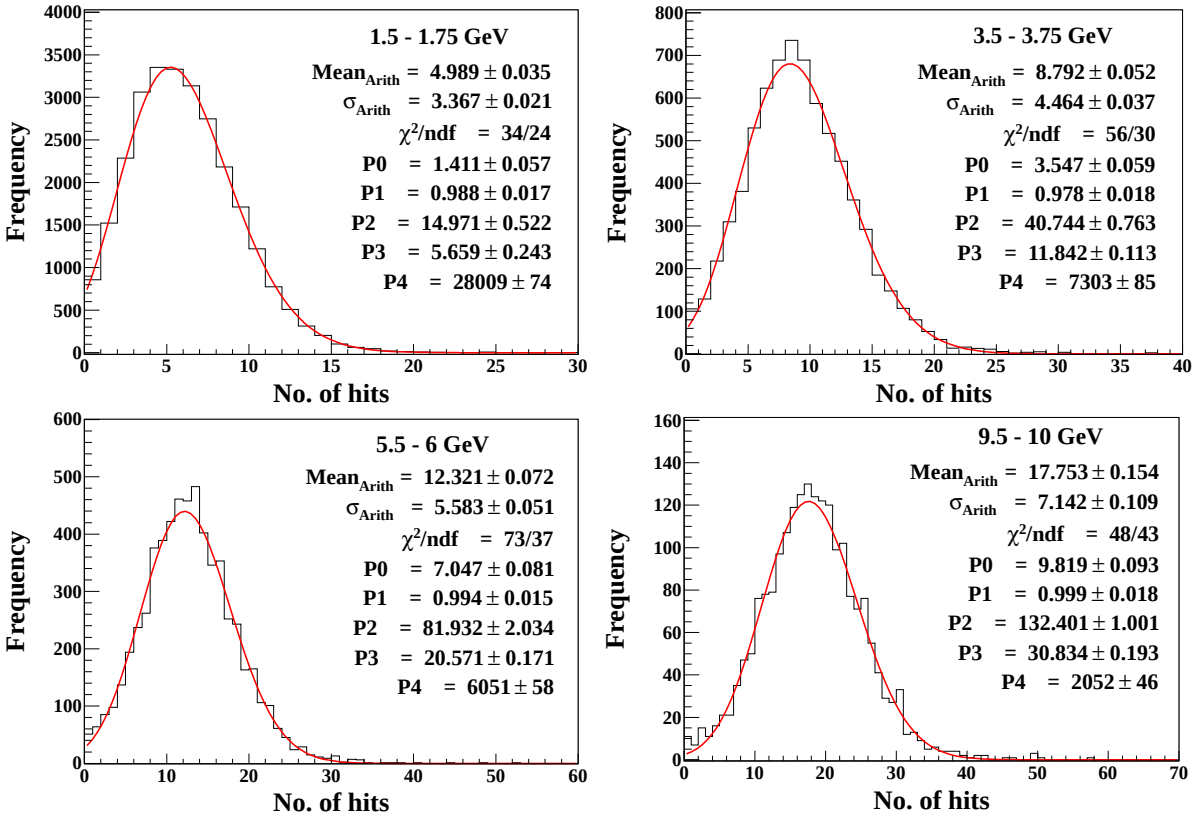

Figure 14: Hadron hit distributions in different E'_{had} energy bins fitted to the Vavilov distribution function in each energy bin.

The four parameters P_i are sufficient to specify the distribution completely and may be directly used in the physics analysis. However, the quantities $mean_{Vavilov}$ and $\sigma_{Vavilov}$ are more useful in intuitively assessing the performance of the detector. The dependence of the $mean_{Vavilov}$ and $\sigma_{Vavilov}$ on energy is shown in Fig. 16.

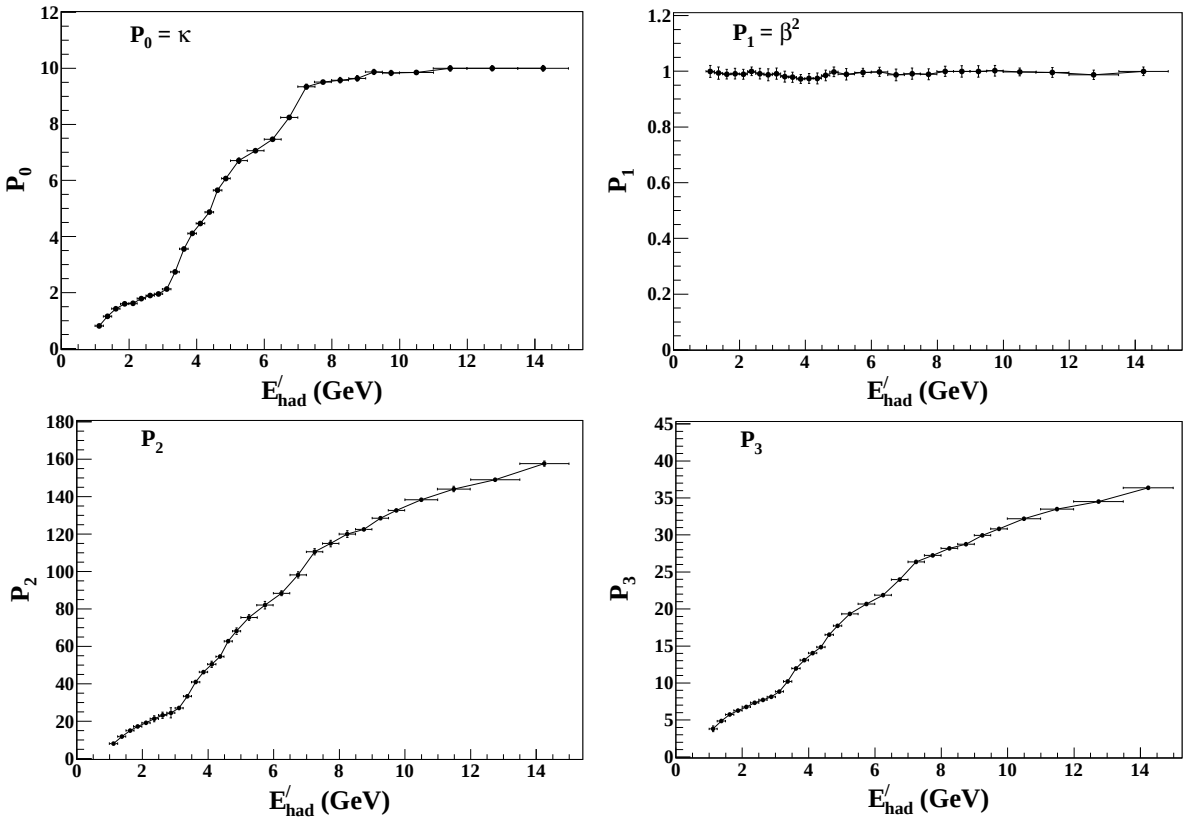

Figure 15: Variation of the Vavilov fit parameters P_0, P_1, P_2, and P_3 with E'_{had} from NUANCE data. The horizontal errors indicate the bin widths.

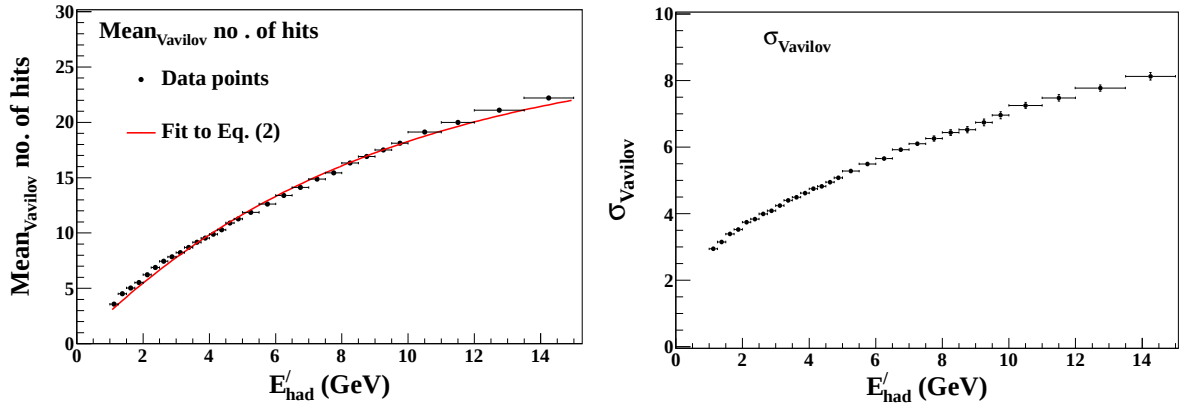

Figure 16: The variations of $\text{mean}_{\text{Vavilov}}$ and σ_{Vavilov} with hadron energy for NUANCE-generated data.

3.2 Dependence of the energy resolution on neutrino oscillations

Note that the effective energy response we obtained from the NUANCE-generated data is an average over the mixture of many hadrons that contribute to hadron shower at all energies. The fractional weights of different kinds of hadrons produced in neutrino interactions may, in principle, depend upon neutrino oscillations. In this section we check if there is any bias in the hadron energy resolution due to oscillations. We use the standard oscillation parameter best-fit values [13] for the mixing angles and mass-squared differences given in Table 4 to generate the events with oscillations. The resolutions obtained without and with oscillations are compared in Fig. 17. As expected, the resolutions are virtually insensitive to oscillations. The marginally higher values of σ/E with oscillations that is seen in the figure is an artifact of the smaller number of events with oscillations.

Δm^2_{21}	$\sin^2 2\theta_{12}$	$\sin^2 2\theta_{13}$	$\sin^2 2\theta_{23}$	Δm^2_{31}
7.6×10^{-5} eV^2	0.86	0.113	1	2.39×10^{-3} eV^2

Table 4: The values of oscillation parameters used in the analysis.

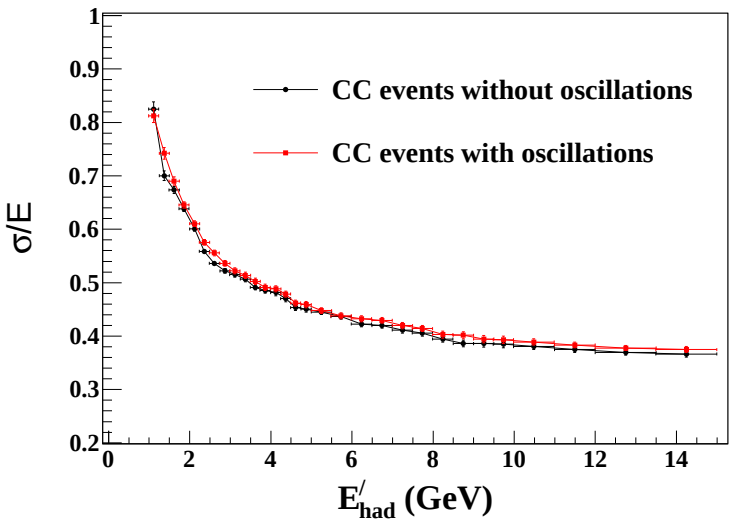

Figure 17: Comparison of energy resolution σ/E of hadrons from charged-current muon neutrino events from oscillated and unoscillated events.

4 Hadron energy calibration from the number of hits

In the previous sections, we have shown the dependence of hadron energy resolution in ICAL on hadron energy. When actual data become available, the hit multiplicity will be known, and the hadron energy E'_{had} will have to be calibrated. We therefore calibrate E'_{had} with respect to the hadron hit multiplicity in a simulated event.

The calibration of the hit multiplicity in terms of the hadron energy not only depends on the detector response discussed above, but also on the energy distribution of hadrons in the detector (that is, the sample of events from oscillated neutrino interactions). To take care of this we have used atmospheric neutrino events generated with the best fit values of the oscillation parameters, as in Table 4, as input to the simulation code. We have checked that changing the oscillation parameters within their current 2σ allowed ranges does not change the results appreciably.

The simulated data were divided into hit_n bins, where hit_n corresponds to n hadron hits. Note that the same number of hits can arise from events with different hadron energies. The distribution of these energies was obtained for each bin, and fitted with the Vavilov distribution. In Fig. 18, the distribution of energy for the bins with 10 and 15 hits are shown.

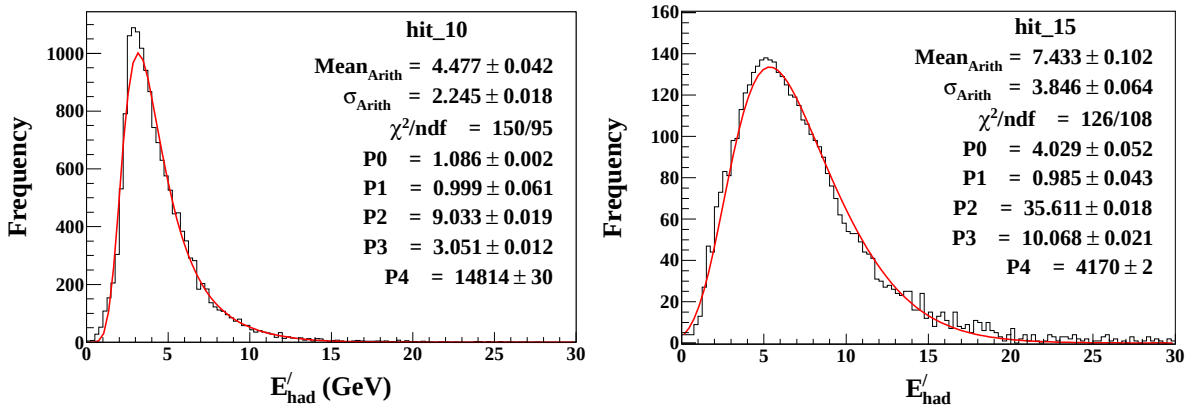

Figure 18: The distribution of hadron energy for (left) 10 hits, and (right) 15 hits.

Fig. 19 shows the calibration plot, with the mean E'_{had} and the error σ obtained from the Vavilov fit. Now from the hit information of the hadron shower in any event in ICAL, we can estimate the hadron energy using this calibration plot. This can then be used to reconstruct the energy and direction of the incident neutrinos.

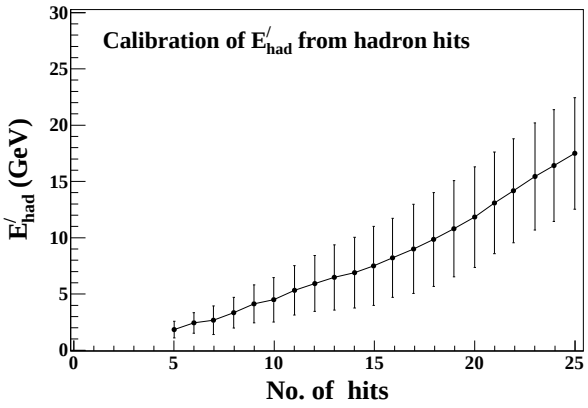

Figure 19: Calibration plot of E'_{had}, where mean and σ from the Vavilov fits are represented by the dots and error bars, respectively.

5 Summary and Conclusions

The ICAL detector is expected to be a good tracking detector for the muons produced in charged current atmospheric ν_μ events. However, in order to reconstruct the neutrino energy, the estimation of the energy of the hadrons produced in such interactions is crucial. Using a GEANT4-based simulations framework of the ICAL detector, we have explored the energy calibration of hadrons from the hadron hit pattern and obtained the hadron energy resolutions.

We now summarize our main results. We have found that the Vavilov distribution function is a good functional form to fit the hadron hit distribution. Analyses, first with fixed-energy pions, and later with a mixture of hadrons from atmospheric ν_μ interaction events, show that a hadron energy resolution in the range (60–40)% at 2–15 GeV is obtainable for hadrons produced in charged-current interactions. We have presented the hadron energy resolution as a function of the incident hadron energy, as well as the calibration plot for the hadron energy, given the hit multiplicity in the detector.

In principle, it is also interesting to study the angular dependence of these resolutions. This will enable the direction of the shower to be determined and will add more information to the reconstruction of the neutrino kinematics. The methodology followed and the issue of the reconstruction of the hadron shower direction will be discussed elsewhere [14].

6 Acknowledgements

The authors thank Gobinda Majumder and Asmita Redij for their contribution in developing the simulation framework for ICAL. One of us (MMD) thanks Tarak Thakore and Meghna K K for discussions on GEANT4 and the NUANCE event generator. We thank Brajesh Choudhary, J.B.Singh and Y.P.Viyogi for the careful reading of the manuscript and the suggestions given in the writing of the paper. We thank Naba Mondal and all other members of INO collaboration for the many constructive suggestions and criticisms given to us.

A The Vavilov distribution function

The Vavilov probability density function in the standard form is defined by

$$P(x;\kappa,\beta^2) = \frac{1}{2\pi i}\int_{c-i\infty}^{c+i\infty}\phi(s)e^{xs}ds, \tag{A.1}$$

where

$$\phi(s) = e^{C}e^{\psi(s)}, \quad C = \kappa(1+\beta^2\gamma) \tag{A.2}$$

and

$$\psi(s) = s\ln\kappa + (s+\beta^2\kappa)\cdot\left[\int_0^1 \frac{1-e^{-st/\kappa}}{t}\,dt \;-\; \gamma\right] - \kappa\, e^{-s/\kappa} \tag{A.3}$$

where $\gamma = 0.5772156649\ldots$ is the Euler's constant. The parameters mean and variance (σ^2) of the distribution in Eq. (A.1) are given by

$$\text{mean} = \gamma - 1 - \ln\kappa - \beta^2; \quad \sigma^2 = \frac{2-\beta^2}{2\kappa}. \tag{A.4}$$

For $\kappa \leq 0.05$, the Landau distribution approximates Vavilov very well while for $\kappa \geq 10$, the Gaussian approximation works well.

We have used the Vavilov pdf which is built into ROOT with the mean shifted from zero. In order to fit the desired distribution the following redefinition of parameters has been adopted: The original Vavilov pdf, that is, $\mathrm{P(x;\ \kappa,\ \beta^2)}$ has been modified to $(\mathrm{P_4/P_3})\ \mathbf{P}(\mathrm{x - P_2/P_3;\ P_0,\ P_1})$. These changes account for normalization ($\mathrm{P_4}$) and the shift of the mean to a non-zero value. This gives the modified mean and variance as

$$\text{Mean} = (\gamma\ -\ 1\ -\ \ln \mathrm{P_0} - \mathrm{P_1})\ \mathrm{P_3} + \mathrm{P_2}; \quad \sigma^2 = (2 - \mathrm{P_1})\ \frac{\mathrm{P_3^2}}{2\mathrm{P_0}}. \tag{A.5}$$

The errors on mean and σ therefore arise from highly correlated parameters P_i. These have been determined from standard analytical formulae [15].

References

[1] M. S. Athar *et al.* [INO Collaboration], "India-based Neutrino Observatory: Project Report. Volume I.," INO-2006-01.

[2] T. Tabarelli de Fatis [MONOLITH Collaboration], hep-ph/0106252; see also, N. Y. Agafonova *et al.* [MONOLITH Collaboration], "MONOLITH: A massive magnetized iron detector for neutrino oscillation studies," LNGS-P26-2000.

[3] F. P. An *et al.* [DAYA-BAY Collaboration], "Observation of electron-antineutrino disappearance at Daya Bay," Phys. Rev. Lett. **108** (2012) 171803 [arXiv:1203.1669 [hep-ex]].

[4] J. K. Ahn *et al.* [RENO Collaboration], "Observation of Reactor Electron Antineutrino Disappearance in the RENO Experiment," Phys. Rev. Lett. **108**, 191802 (2012) [arXiv:1204.0626 [hep-ex]].

[5] Y. Abe *et al.* [DOUBLE-CHOOZ Collaboration], "Indication for the disappearance of reactor electron antineutrinos in the Double Chooz experiment," Phys. Rev. Lett. **108**, 131801 (2012) [arXiv:1112.6353 [hep-ex]].

[6] See http://www.hecr.tifr.res.in/∼ samuel/html/vice.html.

[7] S. Agostinelli *et al.* [GEANT4 Collaboration], "GEANT4: A Simulation toolkit," Nucl. Instrum. Meth. A **506**, 250 (2003), http://geant4.cern.ch/.

[8] R. Brun, F. Rademakers and S. Panacek, "ROOT, an object oriented data analysis framework," For updates and latest version, see http://root.cern.ch/.

[9] D. Casper, "The Nuance neutrino physics simulation, and the future," Nucl. Phys. Proc. Suppl. **112**, 161 (2002) [hep-ph/0208030]; see also, http://nuint.ps.uci.edu/nuance/.

[10] INO collaboration, "A simulations study of the response of ICAL to muons" (in preparation), 2013.

[11] B. Schorr, "Programs for the Landau and the Vavilov distributions and the corresponding random numbers", Comp. Phys. Commm. **7**, 215 (1974); see also, A. Rotondi, P. Montagna, "Fast calculation of Vavilov distribution", Nucl. Instr. & Meth. B 47, 215 (1990).

[12] V. M. Datar, S. Jena, S. D. Kalmani, N. K. Mondal, P. Nagaraj, L. V. Reddy, M. Saraf and B. Satyanarayana *et al.*, "Development of glass resistive plate chambers for INO experiment," Nucl. Instrum. Meth. A **602**, 744 (2009).

[13] J. Beringer et al. (Particle Data Group), Phys. Rev. D 86, 010001 (2012) ; see also [arXiv:1204.0626v2 [hep-ex]].

[14] INO collaboration, "Simulation studies on the hadron shower reconstruction in ICAL", (in preparation), 2013.

[15] Louis Lyons, "Statistics for nuclear and particle physicists", Cambridge University Press, 1986.